Lachmar *et al. Geotherm Energy (2017) 5:28*
https://doi.org/10.1186/s40517-017-0086-8

Geothermal Energy

RESEARCH Open Access

Effect of an 860-m thick, cold, freshwater aquifer on geothermal potential along the axis of the eastern Snake River Plain, Idaho

Thomas E. Lachmar[1*], Thomas G. Freeman[1], Christopher J. Sant[2], Jeffrey R. Walker[3], Joseph F. Batir[4], John W. Shervais[1], James P. Evans[1], Dennis L. Nielson[5] and David D. Blackwell[4]

*Correspondence: tom.lachmar@gmail.com
[1] Department of Geology, Utah State University, Logan, UT 84322-4505, USA
Full list of author information is available at the end of the article

Abstract

A 1912-m exploration corehole was drilled along the axis of the eastern Snake River Plain, Idaho. Two temperature logs run on the corehole display an obvious inflection point at about 960 m. Such behavior is indicative of downward fluid flow in the wellbore. The geothermal gradient above 935 m is 4.5 °C/km, while the gradient is 72–75 °C/km from 980 to 1440 m. Projecting the higher gradients upward to where they intersect the lower gradient on the temperature logs places the bottom of the cold, freshwater Snake River Plain aquifer, which suppresses the geothermal gradient at this location, at least 860 m below the surface. The average heat flow for the corehole between 983 and 1550 m is 132 mW/m^2. Although the maximum bottom-hole temperature extrapolated from a measured time–temperature curve was only 59.3 °C, geothermometers suggest an equilibrium temperature on the order of 125–140 °C based on a single fluid sample from 1070 m. Furthermore, below 960 m the basalt core shows obvious signs of alteration, including a distinct color change, the formation of smectite clay, and the presence of secondary minerals filling vesicles and fracture zones. This alteration boundary could act as an effective cap or seal for a hot-water geothermal system.

Keywords: Corehole, Temperature log, Geothermometers, Basalt, X-ray diffraction

Background

The eastern Snake River Plain (ESRP) in southern Idaho covers an area of approximately 28,000 km^2 (Morse and McCurry 2002), and is a prime target for geothermal exploration due to high geothermal gradients (Blackwell 1989). Heat flow in excess of 100 mW/m^2 has been documented in the area (Blackwell and Richards 2004). This high heat flow is associated with the Yellowstone hotspot, which developed from a mantle plume (Smith et al. 2009). The hotspot was stationary as the North American plate moved southwest over it at a rate of about 2.5 cm/year (Smith and Braile 1994).

The ESRP is home to the Snake River Plain aquifer (SRPA), which is hosted primarily in basalt (Welhan et al. 2002a, b). The majority of these basalts are olivine, tholeiite pahoehoe flows (Greeley 1982; Leeman 1982; Kuntz et al. 1992) with chemical compositions similar to Hawaiian basalts. The bulk of the volcanic vents are clustered around the axis of the ESRP (Kuntz et al. 1992; Smith 2004).

The SRPA is one of the most productive aquifers in the United States (US Geological Survey 1985). The Big Lost River is one of the contributors of recharge to the aquifer (McLing 1994; Orr 1997). However, it is only believed to contribute about 4% of the water input to the system (Ackerman et al. 2010). According to Garabedian (1992), surface-water irrigation is by far the largest contributor, followed by tributary underflow, precipitation, and losses from the Snake River, streams and canals. Discharge from the aquifer is predominantly from irrigation pumping and flow from springs (Mann and Knobel 1990). The average annual discharge at Thousand Springs near Hagerman, Idaho ranges from 3662 million m^3 in 1904 to a high of 6091 million m^3 in 1951 (Bartholomay et al. 2017). Water temperatures range from 6 °C in the northeast to 16 °C at the discharge zone at Hagerman in the southwest (Smith 2004).

Much of the information about the SRPA comes from the Idaho National Laboratory (INL), which is located on the northeastern edge of the aquifer. However, US Geological Survey (USGS) publications provide more inclusive information on the entire ESRPA. The depth to water has been measured from 60 to 270 m below the surface (Ackerman 1991; Knobel et al. 1992). The base of the aquifer has been penetrated in eight deep wells on the INL site, with a depth ranging from 200 to 550 m based on temperature inflections (Smith 2004). The onset of low-temperature alteration identified at the base of the aquifer is thought to control aquifer thickness, and may itself be controlled by thermal flux from below (Morse and McCurry 2002).

A 1912-m geothermal exploration corehole was drilled along the axis of the ESRP near Kimama, approximately 33 km north of Burley, Idaho (Fig. 1). This well, which was cored from 12 m to total depth, is the only deep well in the central SRP to penetrate the base of the aquifer (Shervais et al. 2013, 2014). The Kimama corehole was drilled to establish the nature and thermal history of the central and eastern SRP, and to further the understanding of geothermal systems in southern Idaho (Nielson et al. 2012). Understanding the thermal history can help assess the geothermal energy potential and future needs of geothermal exploration in the ESRP.

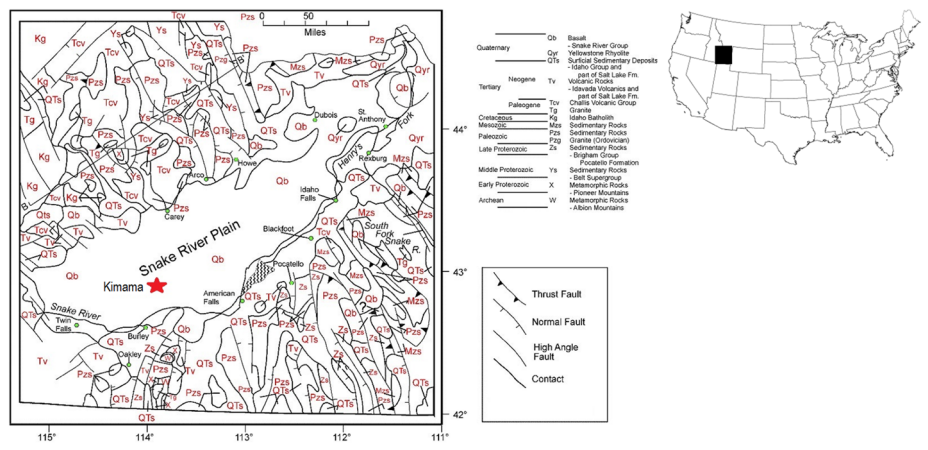

Fig. 1 Project location map. The Kimama drill site is marked with a red star (Adapted from Link et al. (2007))

Methods

The drilling was done by Drilling, Observation, and Sampling of Earth's Continental Crust (DOSECC), a non-profit organization that works in concert with the International Continental Drilling Program (ICDP) on scientific drilling projects such as this one. DOSECC drilled the corehole with an Atlas-Copco CS4002 drilling rig. Drilling commenced on 27 September 2010 and continued through 27 January 2011, when a total depth (TD) of 1912.5 m had been reached (Delahunty et al. 2012). A steel liner was inserted into the well and left to equilibrate for 4 months prior to temperature logging. A separated joint in the liner prevented logging below a depth of 1440 m.

Core logging

Lithologic logging took place as soon as the core reached the surface. Field lithologic logging consisted of washing, measuring, writing a physical description, photographing, and boxing the core. Once boxed, the core was transported offsite for detailed description using the ICDP's Drilling Information System (DIS). The hole was drilled almost entirely through basalt, with thin (2–20 m thick) loess horizons in the upper 365 m and two thick sections of clastic sediments (50–61 m thick) in the lower 200 m. Over 550 basalt flow units were identified (Potter et al. 2011).

Temperature logging

The maximum bottom-hole temperature (BHT) was measured while drilling by DOSECC using a tool that was stored on the top of the core barrel. The core barrel was left on the bottom of the hole for 30 min, and circulation of drilling fluid was halted to minimize disturbances in the hole (Nielson et al. 2012). The resulting time–temperature curves were used to extrapolate to equilibrium temperatures using the $F(\alpha, \tau)$ method (Harris and Chapman 2007). The temperature was measured 25 times, at depths of 520, 660, 700, 731, 937, 1014, 1035, 1059, 1084, 1120, 1139, 1169, 1185, 1221, 1282, 1322, 1364, 1397, 1443, 1492, 1538, 1556, 1586, 1610, and 1824 m (Fig. 2).

Temperature logs were run by the Southern Methodist University (SMU) Geothermal Research Laboratory and the Operational Support Group (OSG) from Helmholtz Centre Potsdam, GeoForschungsZentrum (GFZ), German Research Centre for Geosciences. SMU and OSG used wireline logging tools to record the temperature profile in the well. The SMU tool recorded temperatures while running the tool into the well, and the data had to be downloaded to a computer after the tool had been retrieved from the well. The OSG tool gave live readings and recorded the temperature while pulling the tool out of the hole. The SMU log was acquired on 4 May 2011, while the OSG log was acquired sometime between 29 June and 4 July 2011. Unfortunately, as stated previously, the SMU tool was only able to log to a depth of 1440 m due to a separated joint in the steel liner, while the OSG tool was only able to log to a depth of 1220 m due to subsequent blockage by some unknown cause.

In addition to the temperature log, SMU measured thermal conductivity using the divided-bar method at their Geothermal Laboratory. A detailed explanation of the procedure and tools used is given in Blackwell and Spafford (1987) and is described briefly here. One-inch (2.54 cm) diameter sample plugs from the intervals chosen were collected from the Kimama core and sent to SMU. There, samples were cut to approximately

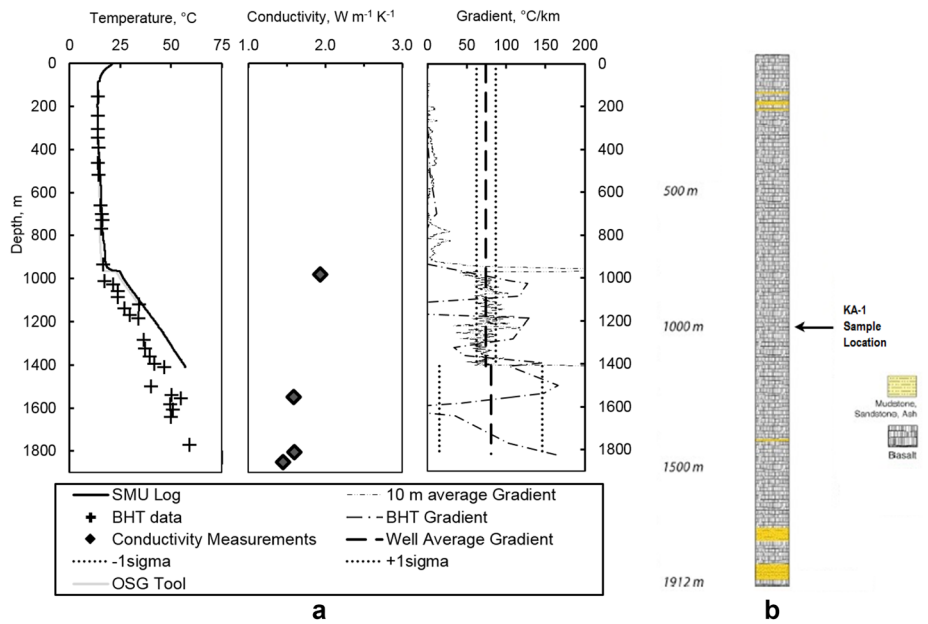

Fig. 2 Temperature logs: **a** SMU, OSG, and DOSECC BHT temperature data, thermal conductivity measurements, and derived gradient, and **b** generalized lithologic log (Adapted from Shervais et al. (2012, 2013))

1.5 in. (3.81 cm) in height, and the tops and bottoms were smoothed to insure proper coupling with the divided-bar apparatus (DBA). Samples were then saturated with water under pressure for 8–12 h. Once saturated, samples were put into the DBA at approximately 400 psi (2760 kPa) with a constant temperature of 25 °C on top and 15 °C on the bottom, forcing a heat flux within the sample. Samples stayed within the DBA until they reached thermal equilibrium, at which point relative thermal conductivity was measured and absolute conductivity was calculated through comparison to standard thermal conductivity samples. Samples were not corrected to in situ conditions because the in situ pressure and temperature impact would be minor and likely within measurement error.

Water sampling

The GFZ fluid sampler is a positive displacement system which allows controlled sampling without sudden decompression or degassing. It can take one sample (0.6 L) at a time. OSG made several attempts to retrieve water plus gas samples from the corehole, but the sampler refused to work properly and only one water sample with no gas phase was collected on 3 July 2011. Due to blockage in the hole, the sampler was not able to get deeper than approximately 1220 m, and the single sample was obtained from only 1070 m.

A water sample was also collected from a shallow, water-supply well nearby. This well was drilled into the SRPA to a TD of about 90 m. There was an electric, submersible pump in this well, and the sample was taken directly from the spigot. In addition, water samples were collected from shallower parts of the corehole as well as from the water-supply well by the USGS (Twining and Barholomay 2011).

Water chemistry

The two water samples were analyzed in the field for temperature, electrical conductivity (EC), pH, and alkalinity. The water samples were analyzed for major and trace ions by ICP (inductively coupled plasma) at the Utah State University Analytical Laboratory (USUAL). Chloride concentrations were determined using a Lachat flow injector analyzer, which is an automated colorimeter. The water samples were also analyzed for the stable isotope ratios of deuterium to hydrogen and ^{18}O to ^{16}O by the Stable Isotope Ratio Facility for Environmental Research (SIRFER) at the University of Utah.

X-ray diffraction

Twenty-two randomly oriented whole-rock sample powders obtained from core were analyzed for clay content and composition using X-ray diffraction from depths of 155, 305, 458, 610, 763, 914, 917, 933, 961, 963, 969, 970, 972, 995, 1005, 1038, 1068, 1221, 1372, 1524, 1676, and 1829 m. In addition, clay separates were analyzed in nine additional samples from the depths of 1042, 1084, 1234, 1311, 1396, 1471, 1676, 1798, and 1829 m. X-ray diffraction analyses were carried out at Utah State University using a Panalytical X'pert Pro X-ray diffraction spectrometer with CuKα radiation at 45 kV and 40 mA. The clay separates were processed in three stages using standard clay identification procedures: air dried, glycolated, and heated at 500 °C for 2 h.

Four samples were also analyzed at Vassar College using a Siemens D-5000 theta:2-theta diffractometer at 40 kV and 30 mA. Clay mineral modeling was completed using the NEWMOD software, 1985 version. NEWMOD is a computer program for the calculation of one-dimensional diffraction patterns of mixed-layered clays.

Results

Geothermal gradients

The maximum BHT was acquired from the DOSECC temperature tool. This tool lies in the core barrel, and thus does not log continuously. However, it was necessary to use this tool throughout the drilling operation because the Idaho Department of Water Resources (IDWR) requires a blowout prevention device if the temperature exceeds 100 °C (Delahunty et al. 2012). The maximum temperature recorded was 59.3 °C at 1824 m, which was the greatest depth at which DOSECC measured the temperature. Because the DOSECC tool was never in true equilibrium with the ambient conditions, the maximum BHT measurement must be lower than the true equilibrium temperature at that depth.

Several methods have been developed for correcting BHT measurements. One of these (Förster 2001) employs a simple empirical correction based on the mean annual ground-surface temperature, the estimated amount of temperature correction at the maximum measurement depth, and the depth of the cross-over point between underestimated temperatures below it and overestimated temperatures above it caused by circulation of drilling fluid. However, the BHT measurements have not been corrected using this, or any other, method because the two temperature logs have been used for determining the geothermal gradients.

Förster (2001) also estimates the average shut-in time necessary for thermal equilibrium to be achieved, which is approximately 1000 h (about 40 days) for wells < 2000 m

deep. Fortunately, the SMU and OSG temperature logs were obtained 97 and 153 to 158 days after drilling had ceased, respectively. Consequently, it has been assumed that these two logs recorded equilibrated temperatures.

The OSG temperature log (Fig. 2) records a geothermal gradient of only 4.5 °C/km above 950 m. The log records a sharp increase in temperature from 16.3 °C at 951 m depth to 23.1 °C at 970 m. The thermal gradient above 950 m is nearly isothermal. This behavior is indicative of downward fluid flow within the wellbore. Due to blockage in the hole, the OSG temperature log only reached a maximum depth of 1131 m, where a temperature of 34.7 °C was measured, resulting in a thermal gradient from 970 to 1131 m of 72 °C/km. This gradient, when projected upward, intersects the shallower, nearly isothermal gradient at approximately 860 m, suggesting that this may be where the bottom of the cold, freshwater SRPA, which suppresses the geothermal gradient at this location, lies.

The SMU temperature log (Fig. 2) reached a maximum depth of 1440 m and displayed a similar profile to the OSG log. Analysis of the temperature–depth curve shows the SRPA perturbing the geothermal gradient from 0 to 935 m. Below 1000 m, the temperature log has a nearly linear 10-m averaged gradient of 75 ± 12 °C/km. The high 1sigma within the gradient is likely an artifact of the high depth resolution of the temperature log, which introduces large gradient swings for minor changes in temperature. A 10-m average was applied to the gradient to remove some of this noise. The gradient varied from approximately 40 °C/km to greater than 100 °C/km even after the 10-m average was applied. When this higher gradient is projected upward, it also intersects the low, shallower gradient at about 860 m. The temperature at TD (1912 m), projected downward, would be approximately 94 °C. The DOSECC BHT temperature data produce a similar average gradient, but had higher error and were not used for the subsequent heat-flow calculation. There are two major gradient spikes at about 970 and 1410 m (Fig. 2) that may indicate high permeability zones.

The SMU temperature data were combined with thermal conductivity measurements of core samples to calculate heat flow (Fig. 2). Core photographs were inspected and samples were chosen to represent major basalt flow units between 900 and 1900 m. In all, six rock samples were sent to SMU for thermal conductivity measurements. One sample broke; consequently, thermal conductivity was measured only once for three of the five rock samples, and only twice for the other two samples (Table 1). Thermal conductivity decreases slightly from 1000 to 1900 m, which is likely related to the increase in thermal alteration with depth, although a drop in conductivity did not produce a

Table 1 Thermal conductivity measurements from core

Depth (m)	Thermal conductivity (W m^{-1} K^{-1})	Number of sample runs
983	1.93 ± 0.00	2
1550	1.59	1
1807	1.60	1
1854	1.45	1
1902	1.09 ± 0.01	2

statistically significant change in thermal gradient, suggesting that conductivity is relatively constant throughout the measured section.

Samples at 983 and 1550 m were averaged to calculate a mean conductivity for the section with a measured thermal gradient. The average gradient for the measured thermal regime is 1.76 ± 0.2 W m^{-1} K^{-1}. The thermal conductivity values below 1550 m were not used in the average conductivity because the thermal regime of this section is only characterized by BHT measurements, which show greater variability and potential error than the section above. The lower thermal conductivity measurements are expected to represent a change in rock properties, which would also be indicated in the temperature log through a change in the geothermal gradient, but there would be a constant heat flow throughout the well. Using the deeper thermal conductivity measurements would introduce unnecessary error since there is not an equally deep equilibrium thermal gradient to use for heat flow calculation. The average heat flow is 132 ± 26 mW/m^2 calculated using the thermal gradient from 1000 to 1400 m, and the average thermal conductivity for samples at 983 and 1550 m. This value is statistically the same as other deep wells in the SRP (Blackwell 1989), and is thus considered representative of background regional heat flow.

Water chemistry

The results of the field and chemical analyses of the two water samples are given in Table 2. KA-W is the sample from the 91-m deep water-supply well. KA-1 is the sample from the corehole at a depth of 1070 m. The temperature of the KA-1 sample is not representative of the temperature at 1070 m due to the amount of time between when the sample was captured and when the temperature was measured at the surface. For this reason, the temperature logs will be used to analyze the temperature of the water in the corehole.

The pH values of the two water samples are similar, with both being mildly alkaline. However, the electrical conductivity (EC) in the corehole water is about three times greater than in the water-supply well. Furthermore, the KA-W sample is calcium–magnesium–bicarbonate water, while the KA-1 sample is sodium–chloride water. These differences are to be expected considering the depths from which the samples were taken.

The chemical analysis of the KA-1 water sample is also shown in two geothermal plots developed by Giggenbach (1988). The first discriminates between: (1) fully equilibrated (2) partially equilibrated, and (3) immature waters. The KA-1 sample plots on the bottom line of being partially equilibrated (Fig. 3). The second technique developed by Giggenbach (1988) is to plot the chloride, sulfate, and bicarbonate concentrations on a triangular diagram. Acid, neutral chloride, and soda springs waters are the three broad

Table 2 Results of chemical analyses of KA-W and KA-1 water samples (all units in mg/L unless otherwise noted)

Sample	T (°C)	EC (µS)	pH	Alkalinity	Ca	Mg	Na	K	Cl	SO_4	SiO_2
KA-W	15.8	336	7.71	160	25.0	12.7	16.5	3.60	13.1	22.1	60.9
KA-1	28.8	1060	8.17	120	21.1	3.21	284	10.3	315	306	158

Ion balance errors = 5.3% for KA-W and 9.5% for KA-1

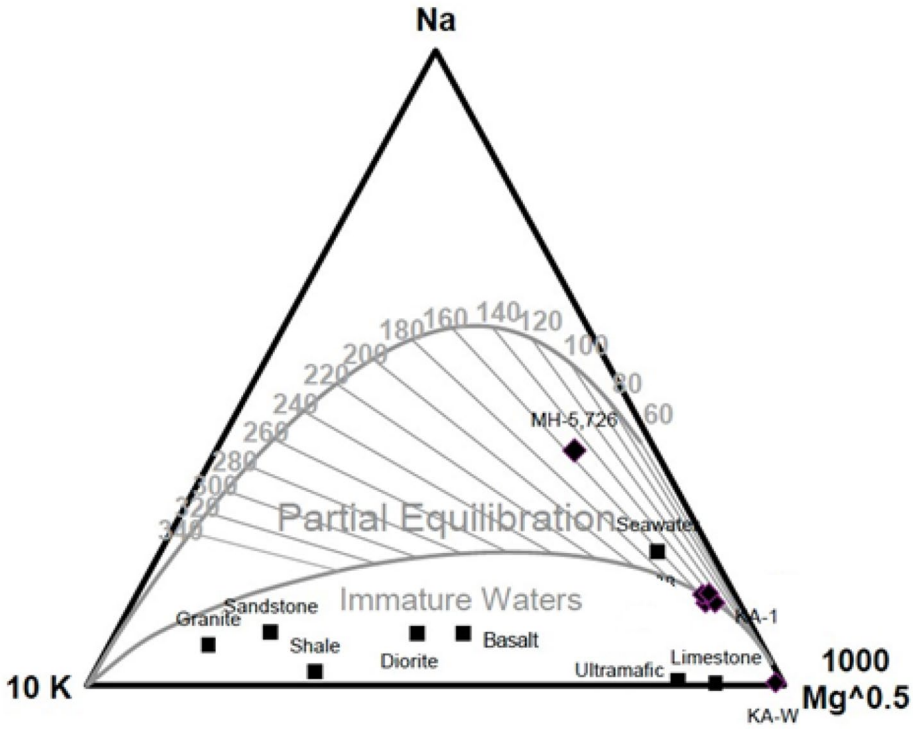

Fig. 3 KA-1 and KA-W samples plotted on Giggenbach (1988) triangular graph

classification types. The KA-1 sample plots close to the neutral chloride/acid water boundary (Fig. 4).

Results of the stable isotopic analyses are displayed in Fig. 5. Comparison to the global meteoric water line (GMWL) (Craig 1961) shows that both samples plot very close to the GMWL. This indicates that both samples are meteoric waters. However, because sample KA-1 was taken from a relatively shallow depth, it may not be representative of deeper geothermal waters. Nonetheless, because a steel liner was inserted into the hole upon completion of the drilling, which became separated at 1440 m prior to sampling, it seems possible that the KA-1 sample may actually be representative of the water at that depth or at the bottom of the hole.

Geothermometers

Geothermometers are temperature indicators using temperature dependent geochemical and/or isotopic compositions of geothermal waters (Gupta and Roy 2007). All geothermometers have limitations. The following assumptions are made when using geothermometers: (1) the relevant hydrothermal minerals in the reservoir are in equilibrium with the geothermal liquid; (2) the pore fluid pressure in the reservoir is fixed by coexistence of liquid and steam; (3) the geothermal liquid cools, either conductively or adiabatically, through steam separation at 100 °C; (4) the geothermal liquid does not mix with cold, shallow waters during the ascent towards the surface; (5) the geothermal liquid does not precipitate any relevant minerals along the upflow path (Marini 2004).

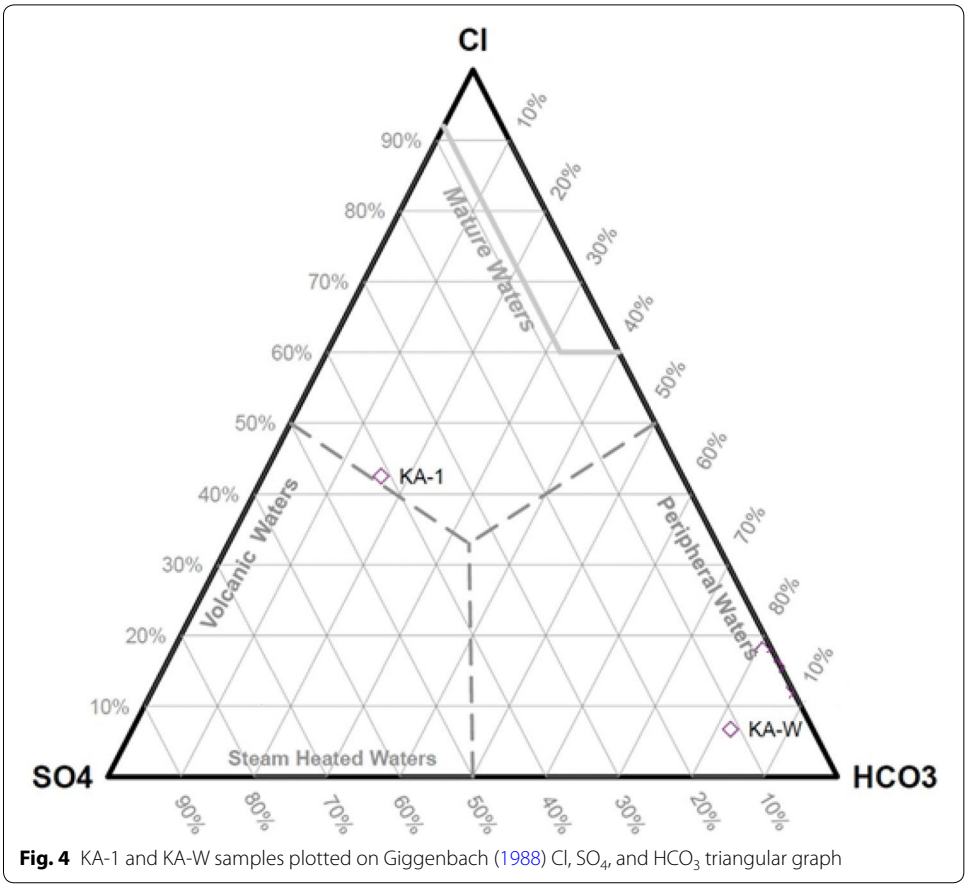

Fig. 4 KA-1 and KA-W samples plotted on Giggenbach (1988) Cl, SO_4, and HCO_3 triangular graph

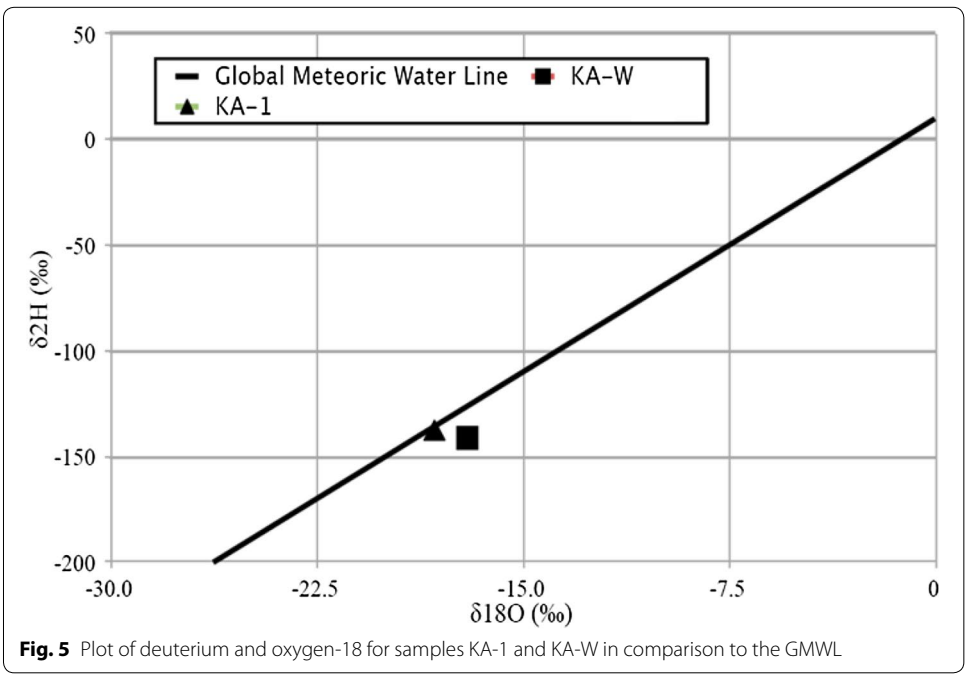

Fig. 5 Plot of deuterium and oxygen-18 for samples KA-1 and KA-W in comparison to the GMWL

In most situations it is difficult to prove that these assumptions are met (Ferguson et al. 2009).

A range of elemental geothermometers was applied to the KA-1 water sample: chalcedony and quartz (Fournier 1973, 1977), Na/K (Fournier 1979), Na/K (Giggenbach 1988), Na–K–Ca (Fournier and Truesdell 1973), Na–K–Ca–Mg (Fournier and Potter 1979), and K^2/Mg (Giggenbach 1988). The KA-1 water sample was not analyzed for Li, so geothermometers such as Na/Li and Mg/Li (Kharaka and Mariner 1989) could not be applied.

Equilibrium reservoir temperatures calculated for KA-1 are summarized in Table 3. Six of the seven geothermometers predict equilibrium temperatures above 125 °C. The quartz (Fournier 1977) and Na/K (Giggenbach 1988) geothermometers predict equilibrium temperatures above 160 °C. The Na–K–Ca (Fournier and Truesdell 1973) geothermometer provides a result of 139 °C. The KA-1 sample has a magnesium concentration of 3.21 mg/L (Table 2), and when the correction is applied (Fournier and Potter 1979) the estimated equilibrium temperature drops to only 125 °C. All of these geothermometers may have been affected by mixing with shallow groundwater from the SRPA due to the relatively shallow depth from which the sample was taken, so these temperatures might only reflect minimum reservoir temperatures for the underlying geothermal system.

Physical description of core

The core contains 557 flow units (Potter 2014). The unaltered basalts are a light gray, commonly diktytaxitic to intergranular textured, olivine tholeiites, very similar to the basalts at the INL described by Morse and McCurry (2002). Vesicles are concentrated just below the flow unit tops typically, but also form vesicle columns or trains locally. Phenocrysts of plagioclase and olivine exist within a fine-grained matrix of plagioclase, pyroxene, and glass. Phenocryst content ranges from about 10 to 20%, and vesicle content ranges from ≤ 5 to 50%. Most vesicles above 970 m do not contain authigenic minerals, although large irregular gas cavities, which are much larger than the surrounding vesicles, are commonly lined with calcite with or without quartz.

Below 970 m vesicles are commonly lined with calcite or smectite-group clay minerals (green-brown nontronite or blue saponite). Below 1200 m many vesicles are filled with either blue saponite or calcite plus quartz (with calcite lining the walls and quartz filling the interiors). Rare zeolite fillings were observed around 1400 m depth. The shallowest depth at which all vesicles are filled is 1042 m. The greatest depth at which open vesicles are observed is 1833 m.

The color of the core changes with depth. Fresh, unaltered basalts are gray in color, with a few reddish, oxidized zones. A rapid color change from gray to green or

Table 3 Geothermometer calculations for KA-1 (all values in °C)

Sample	Chalcedony[a]	Quartz[a]	Na/K[b]	Na/K[c]	Na–K–Ca[d]	Na–K–Ca–Mg[e]	K^b/Mg[c]
KA-1	141	164	143	163	139	125	80.2

[a] Fournier (1977)

[b] Fournier (1979)

[c] Giggenbach (1988)

[d] Fournier and Truesdell (1973)

[e] Fournier and Potter (1979)

Fig. 6 Core from 1009 to 1014 m. Basalts are still gray with open vesicles, and no authigenic minerals are present

Fig. 7 Core from 1025 to 1028 m. Basalts have a greenish tint as well as clay deposition and other secondary minerals filling vesicles and fractures

red–brown occurs at about 1020 m (Figs. 6, 7). The deepest basalts (> 1800 m depth) are thoroughly altered to greenish black with red streaks.

X-ray diffraction

Twenty-two whole-rock powders were analyzed using X-ray diffraction. The samples were chosen to avoid vesicle fillings and include only basalt groundmass. The shallowest occurrence of clay in the basalt groundmass is in the sample from 963 m; clay peaks are not present in any of the nine samples above 963 m. All seven samples below 1038 m have clay peaks present. Two of the five samples between 963 and 1038 m show a clay peak (at 969 and 972 m), while three do not (at 970, 995, and 1005 m).

Nine clay separate samples were analyzed using X-ray diffraction. Clay separate samples were taken starting at 1042 m because that is the approximate depth at which clays become abundant enough in the groundmass to collect a sufficient amount of material for X-ray analysis. The X-ray diffraction results indicate the presence of smectite clay in the core. The presence of smectite is expected because it has been found in basalts at the INL (Morse and McCurry 2002) and in Hawaiian basalts (Tomasson and Smarason 1985), both of which are very similar geochemically to the basalts at Kimama.

Smectites from the core are both dioctahedral and trioctahedral. The NEWMOD modeling suggests that two of the samples (at 1234 and 1798 m) are dioctahedral smectites. The samples from 1042, 1471, 1676, and 1829 m may also be interpreted as dioctahedral smectites. Dioctahedral clays are formed from weathering of potassium feldspars and are commonly found in sedimentary rocks. Sedimentary interbeds were observed a short distance from the samples from 1042 and 1234 m, so it is expected that they are dioctahedral.

X-ray diffraction data reveal that the sample from 1396 m is a trioctahedral smectite. The samples from 1084 and 1311 m may also be interpreted as trioctahedral smectites. Trioctahedral clays are derived from the weathering of mafic minerals, such as basaltic glass.

With increasing temperature, dioctahedral smectites convert to illite. Trioctahedral clays convert to chlorite instead of illite with increasing temperature and pressure. Johnston (1983) suggests that the temperature at which dioctahedral smectite begins to become unstable and convert to illite is 90 °C. Six of the nine samples analyzed are interpreted as dioctahedral smectites. Also, smectites should become unstable at generally the same conditions whether they are dioctahedral or trioctahedral. Finally, no mixed-layer clays of smectite/illite or smectite/chlorite were observed. Therefore, the temperature since the formation of the smectite clays has remained below 90 °C. This is consistent with the maximum temperatures recorded for each of the three temperature logs, the highest of which was 59.3 °C for the DOSECC temperature tool, as well as the temperature at TD projected downward from the SMU temperature log of 94 °C.

Discussion

Three separate observations—the temperature logs, the physical characteristics of the core, and the mineralogical data from the X-ray diffraction analyses—all suggest that a major boundary between unaltered and altered basalts is present in the axial zone of the SRP at Kimama between about 860–970 m below the surface. First, the temperature

logs exhibit a sharp inflection point at around 960 m, with a near isothermal gradient of 4.5 °C above 935–950 m and a conductive gradient of 72–75 °C below 970–980 m. This behavior is indicative of downward fluid flow in the wellbore, and projecting the higher gradients upward to their intersection with the lower gradient on the temperature logs places the bottom of the cold, freshwater SRPA at approximately 860 m.

Second, the basalts above 950 m show no signs of alteration. Between 970 and 1020 m, the core shows a gradational change from fresh to altered basalts. All basalts below 1020 m show signs of alteration that become more significant with depth. Clays first begin to appear as vesicle linings around 950 m depth. The color of the core remains light gray, then changes abruptly at about 1020 m, where it becomes greenish–gray, and the vesicles begin to be filled with clay minerals (nontronite, saponite), calcite, quartz, and more rarely zeolites. Finally, mineralogical data from the X-ray diffraction analyses suggest that the first signs of groundmass alteration occur at around 960 m with the appearance of smectite clays in the basalts.

All three observations point to clogging of the basalt pore spaces to create a natural boundary between the relatively fast moving, cold fresh water above 860 m depth, and little or no moving water below 970 m depth. Morse and McCurry (2002), Smith (2004), and McLing et al. (2016) have made similar observations at other locations on the ESRP, but at shallower depths. Based on these data, the base of the SRPA in the axial zone at Kimama is at least 860 m below the surface. This is 1.6–4.3 times greater than the estimated base of the SRPA on the INL site (McLing et al. 2002, 2016; Morse and McCurry 2002; Smith 2004).

Conclusions

The highest temperature recorded by DOSECC in the corehole was 59.3 °C at a depth of 1824 m. The geothermal gradient was only 4.5 °C/km above 935 m, but increased dramatically to 72–75 °C/km below 980 m. Extrapolating this gradient, the projected temperature at TD would be approximately 94 °C. This is consistent with the observation that the temperature since the formation of the smectite clays, the deepest sample of which was obtained from core at 1829 m, has remained below 90 °C. The suppression of the gradient above 860 m is due to the cold, fresh water of the SRPA (e.g., Smith 2004). Furthermore, the swelling smectite clays clog pore spaces in the basalts, creating a natural seal for rising thermal waters below the SRPA.

Results of the chemical analyses of the water samples show that there is a distinction between the deeper geothermal waters (KA-1) and the shallow SRPA water (KA-W). KA-1 is characterized as a sodium-chloride water, while KA-W is a calcium–magnesium-bicarbonate water. The stable isotopic compositions of KA-1 and KA-W indicate that they both are meteoric waters. If the geothermal waters are indeed meteoric, then they have moved down flow paths to these relatively great depths and have begun equilibrating with the geothermal system.

Geothermometers suggest that the deeper waters mixed into the system reach higher temperatures than were actually recorded in the corehole. The Na–K–Ca geothermometer (Fournier and Truesdell 1973) results in an estimate of 139 °C. However, this geothermometer gives inconsistent results for temperatures below 200 °C (Paces 1975). Because the temperature is below 200 °C, the Na–K–Ca–Mg geothermometer (Fournier

and Potter 1979) should provide better results. This geothermometer gives an estimate of 125 °C, suggesting that there are magnesium reactions taking place which affect the geothermometer estimates.

The alteration boundary at 950 to 970 m could act as an effective cap or seal for a hot-water geothermal system. Such a system ranges in water temperatures from 50 to 150 °C (Gupta and Roy 2007).

The geothermal resource in the axial zone of the ESRP warrants further exploration. Although it could be debated whether this resource is economically reasonable in this area, well depths in excess of 2 km should yield sufficiently high temperatures to cause the conversion of smectite clays to illite, which would enhance fluid flow. Furthermore, the same caliber of geothermal resources may be found closer to the surface along the margins of the ESRP where the aquifer is thinner, thereby decreasing the depth of drilling and the initial cost of geothermal exploration.

Authors' contributions

TEL and TGF collected the water samples and interpreted the results of their chemical analyses. CJS and JWS logged the core samples, and CJS and JRW analyzed the core samples using X-ray diffraction. JFB made the thermal conductivity measurements and heat flow calculation. JWS and JPE served as the principal investigators. DDB and DLN obtained and interpreted two of the three temperature logs. All authors read and approved the final manuscript.

Author details

[1] Department of Geology, Utah State University, Logan, UT 84322-4505, USA. [2] Department of Earth Sciences, Syracuse University, Syracuse, NY 13244, USA. [3] Department of Earth Science & Geography, Vassar College, Poughkeepsie, NY 12604, USA. [4] Department of Earth Sciences, Southern Methodist University, Dallas, TX 75275-0395, USA. [5] DOSECC Exploration Services, LLC, 2075 Pioneer Road, Salt Lake City, UT 84104, USA.

Acknowledgements

This work is part of Project HOTSPOT, an ARRA (American Recovery and Reinvestment Act) project funded by US Department of Energy award DE-EE0002848, the International Continental Drilling Program, and Utah State University, with additional support from the Snake Play Fairway project (DE-EE0006733). The authors also thank the two anonymous reviewers and editor Olaf Kolditz, whose insights and suggestions greatly improved the final version of this work.

Competing interests

The authors declare that they have no competing interests.

Ethics approval and consent to participate

Not applicable.

Availability of data and materials

The datasets supporting the conclusions of this article are available in the Utah State University Libraries Digital Commons repository at http://digitalcommons.usu.edu/.

Publisher's Note

Received: 12 July 2017 Accepted: 6 December 2017
Published online: 15 December 2017

References

Ackerman DJ. Transmissivity of the Snake River Plain aquifer at the Idaho National Engineering Laboratory, Idaho. US Geological Survey Water-Resources Investigations Report 91-4058 (DOE/ID-22097); 1991. p. 1–35.

Ackerman DJ, Rousseau JP, Rattray GW, Fisher JC. Steady-state and transient models of groundwater flow and advective transport, eastern Snake River Plain aquifer, Idaho National Laboratory and Vicinity, Idaho. US Geological Survey Scientific Investigations Report 2010-5123; 2010. p. 1–220.

Bartholomay RC, Maimer NV, Rattray GW, Fisher JC. An update of hydrologic conditions and distribution of selected constituents in water, eastern Snake River Plain aquifer and perched groundwater zones, Idaho National Laboratory, Idaho, emphasis 2012–15. US Geological Survey Scientific Investigations Report 2017-5021; 2017. p. 1–87.

Blackwell DD. Regional implications of heat flow of the Snake River Plain, northwestern United States. Tectonophysics. 1989;164:323–43.

Blackwell DD, Richards M. Geothermal map of North America. American Association of Petroleum Geologists. 2004. (scale 1:6,500,000).

Blackwell DD, Spafford RE. Experimental methods in continental heat flow. In: Sammis CG, Henyey TL, editors. Experimental methods in physics—Geophysics, part B—field measurements, 24. Cambridge: Academic Press; 1987. p. 189–26.
Craig H. Isotopic variations in meteoric waters. Science. 1961;133:1702–3.
Delahunty C, Nielson DL, Shervais JW. Coring of three deep geothermal holes, Snake River Plain, Idaho. Geotherm Res Counc Trans. 2012;36:641–7.
Ferguson G, Grasby SE, Hindle SR. What do aqueous geothermometers really tell us? Geofluids. 2009;9:39–48.
Förster A. Analysis of borehole temperature data in the Northeast German Basin: continuous logs versus bottom-hole temperatures. Pet Geosci. 2001;7:241–54.
Fournier RO. Silica in thermal waters: Laboratory and field investigations. Biogeochemistry. 1973. p. 122–39.
Fournier RO. Chemical geothermometers and mixing models for geothermal systems. Geothermics. 1977;5:41–50.
Fournier RO. A revised equation for Na–K geothermometer. Geotherm Res Counc Trans. 1979;3:221–4.
Fournier RO, Potter RW. Magnesium correction to the Na–K–Ca chemical geothermometer. Geochim Cosmochim Acta. 1979;43:1543–50.
Fournier RO, Truesdell A. An empirical Na–K–Ca geothermometer for natural waters. Geochim Cosmochim Acta. 1973;37:1255–75.
Garabedian SP. Hydrology and digital simulation of the regional aqifer system, eastern Snake River Plain, Idaho. US Geological Survey Professional Paper 1408-F; 1992. p. 1–102.
Giggenbach WF. Geothermal solute equilibria: derivation of Na–K–Mg–Ca geoindicators. Geochim Cosmochim Acta. 1988;52:2749–65.
Greeley R. The style of basaltic volcanism in the eastern SRP, Idaho. In: Bonnichsen B, Breckenridge RM, editors. Cenozoic Geology of Idaho. Idaho Bureau of Mines and Geology Bulletin 26; 1982. p. 407-21.
Gupta HK, Roy S. Geothermal energy: an alternative resource for the 21st century. Amsterdam: Elsevier; 2007.
Harris RN, Chapman DS. Stop-go temperature logging for precision applications. Geophysics. 2007;72:E119–23.
Johnston RM. The conversion of smectite to illite in hydrothermal systems: a literature review. Atomic Energy of Canada Limited; 1983. (ACEL-7792).
Kharaka Y, Mariner R. Chemical geothermometers and their application to formational waters from sedimentary basins. In: Naeser ND, McCulloch T, editors. Thermal history of sedimentary basins: methods and case histories. New York: Springer Verlag; 1989. p. 99–117.
Knobel LL, Bartholomay L, Dewayne C, Tucker BJ, Wegner SJ. Chemical constituents in the dissolved and suspended fractions of the groundwater from selected sites. US Geological Survey Open-File Report 92–51; 1992. p. 1–56.
Kuntz MA, Covington HR, Schorr LJ. An overview of basaltic volcanism of the eastern Snake River Plain, Idaho. In: Regional geology of eastern Idaho and western Wyoming. Boulder: Geological Society of America Memoir 179; 1992. p. 227–67.
Leeman WP. Olivine tholeiitic basalts of the SRP, Idaho. In: Bonnichsen B, Breckenridge RM, editors. Cenozoic geology of Idaho. Idaho Bureau of Mines and Geology Bulletin 26; 1982. p. 181–91.
Link PK, Lewis RS, Khan S, Schmidt K, Ames D. Digital geology of Idaho—Basin & range province—Tertiary extension. Geology 456–556, module 9. Pocatello: Idaho State University; 2007.
Mann LJ, Knobel LL. Radionuclides, metals, and organic compounds in water, eastern part of A & B Irrigation District, Minidoka County, Idaho. US Geological Survey Open-File Report 90-191 (DOE/ID-22087); 1990. p.1–36.
Marini L. Geochemical techniques for the exploration and exploitation of geothermal energy. Genova: Universita degli di Genova; 2004.
McLing TL. The Pre-anthropogenic groundwater evolution at the Idaho National Engineering Laboratory site, Idaho. MSc Thesis. Pocatello: Idaho State University; 1994.
McLing TL, Smith R, Johnson TM. Chemical characteristics of thermal water beneath the eastern SRP. In: Link PK, Mink LL, editors. Geology, hydrogeology, and environmental remediation: Idaho National Engineering and Environmental Laboratory, eastern Snake River Plain, Idaho. Boulder: Geological Society of America Special Paper 353; 2002. p. 205–11.
McLing TL, Smith RP, Smith RW, Blackwell DD, Roback RC, Sondrup AJ. Wellbore and groundwater temperature distribution eastern Snake River Plain, Idaho: implications for groundwater flow and geothermal potential. J Volcanol Geoth Res. 2016;320:144–55.
Morse LH, McCurry M. Genesis of alteration of quaternary basalts within a portion of the eastern SRP aquifer. In: Link PK, Mink LL, editors. Geology, hydrogeology, and environmental remediation: Idaho National Engineering and Environmental Laboratory, eastern Snake River Plain, Idaho. Boulder: Geological Society of America Special Paper 353; 2002. p. 213–24.
Nielson DL, Delahunty C, Shervais JW. Geothermal systems in the Snake River Plain, Idaho, characterized by the Hotspot Project. Geotherm Res Counc Trans. 2012;36:727–30.
Orr BR. Geohydrology of the Idaho National Engineering and Environmental Laboratory, eastern Snake River Plain, Idaho. US Geological Survey Fact Sheet FS-130-97; 1997.
Paces T. A systematic deviation from Na–K–Ca geothermometer below 75 °C and above 10–4 atm Pco2. Geochim Cosmochim Acta. 1975;39:541–4.
Potter KE, Bradshaw R, Sant CJ, King J, Shervais JW, Christiansen E. Project Hotspot: insight into the subsurface stratigraphy and geothermal potential of the Snake River Plain. Geotherm Res Counc Trans. 2011;35:967–71.
Potter KE. The Kimama core: A 6.4 Ma record of volcanism, sedimentation, and magma petrogenesis on the axial volcanic high, Snake River Plain, ID. PhD Dissertation. Logan: Utah State University; 2014.
Shervais JW, Nielson D, Evans JP, Lachmar TE, Christiansen E, Morgan L, Shanks WCP, Delahunty C, Schmitt DR, Liberty LM, Blackwell DD, Glen JM, Kessler JE, Potter KE, Jean MM, Sant CJ, Freeman TG. Hotspot: the Snake River Plain geothermal drilling project—initial report. Geotherm Res Counc Trans. 2012;36:767–72.
Shervais JW, Schmitt DR, Nielson DL, Evans JP, Christiansen EH, Morgan L, Shanks WCP, Lachmar T, Liberty LM, Blackwell DD, Glen JM, Champion D, Potter KE, Kessler JA. First results from HOTSPOT: the Snake River Plain scientific drilling project, Idaho, USA. Sci Drill. 2013;15:36–45.

Shervais JW, Evans JP, Schmitt D, Christiansen EH, Prokopenko A. HOTSPOT: the Snake River scientific drilling project. EOS Trans Am Geophys Union. 2014;95:85–6.
Smith RB. Geologic setting of the Snake River Plain aquifer and vadose zone. Vadose Zone J. 2004;3:47–58.
Smith RB, Braile LW. The Yellowstone hotspot. J Volcanol Geoth Res. 1994;61:121–87.
Smith RB, Jordan M, Steinberger B, Puskas CM, Farrell J, Waite GP, Husen S, Chang W, O'Connell R. Geodynamics of the Yellowstone hotspot and mantle plume: seismic and GPS imaging, kinematics, and mantle flow. J Volcanol Geoth Res. 2009;188:26–56.
Tomasson J, Smarason OB. Developments in geothermal energy. In: Jones GP, Downing RA, editors. Hydrogeology in the service of man. Proceedings International Association of Hydrogeologists, Cambridge. 1985. p. 8–13.
Twining BV, Bartholomay RC. Geophysical logs and water-quality data collected for boreholes Kimama-1A and -1B, and a Kimama water supply well near Kimama, southern Idaho. US Geological Survey Data Series 622 (DOE//ID 22215); 2011. p. 1–18 (plus appendix).
US Geological Survey. National water summary, 1984: Hydrologic events, selected water-quality trends, and ground-water resources. US Geological Survey Water-Supply Paper 2275. 1985. p.1–467.
Welhan JA, Johannesen CM, Davis LL, Reeves KS, Glover JA. Overview and synthesis of lithologic controls on aquifer heterogeneity in the eastern Snake River Plain, Idaho. In: Bonnichsen B, White C, McCurry M, editors. Tectonic and magmatic evolution of the Snake River Plain volcanic province. Idaho Geological Survey Bulletin 30; 2002a. p. 455–60.
Welhan JA, Johannesen CM, Reeves KS, Clemo TM, Glover JA, Bosworth KW. Morphology of inflated pahoehoe lavas and spatial architecture of their porous and permeable zones, eastern SRP, Idaho. In: Link PK, Mink LL, editors. Geology, hydrogeology, and environmental remediation: Idaho National Engineering and Environmental Laboratory, eastern Snake River Plain, Idaho. Boulder: Geological Society of America Special Paper 353; 2002b. p. 135–50.